

Optimization of the beam quality in ionization injection by a tailoring gas profile

Ye Cui(崔野), Guo-Bo Zhang(张国博), Yan-Yun Ma(马燕云), Xiao-Hu Yang(杨晓虎), Jia-Yin Mu(牟佳胤), Hai-Bo Yao(姚海波), Ming Zi(资明), Jie Zhou(周洁), Jing-Qi Yang(杨静琦), Li-Xiang Hu(胡理想), and Li-Chao Tian(田立朝)

Citation: Chin. Phys. B, 2021, 30 (**10**): 105201. DOI: 10.1088/1674-1056/ac1b89
Journal homepage: http://cpb.iphy.ac.cn; http://iopscience.iop.org/cpb

What follows is a list of articles you may be interested in

Laser-driven relativistic electron dynamics in a cylindrical plasma channel

Pan-Fei Geng(耿盼飞), Wen-Juan Lv(吕文娟), Xiao-Liang Li(李晓亮), Rong-An Tang(唐荣安), Ju-Kui Xue(薛具奎)
Chin. Phys. B, 2018, 27 (**3**): 035201. DOI: 10.1088/1674-1056/27/3/035201

Acceleration and radiation of externally injected electrons in laser plasma wakefield driven by a Laguerre-Gaussian pulse

Zhong-Chen Shen(沈众辰), Min Chen(陈民), Guo-Bo Zhang(张国博), Ji Luo(罗辑), Su-Ming Weng(翁苏明), Xiao-Hui Yuan(远晓辉), Feng Liu(刘峰), Zheng-Ming Sheng(盛政明)
Chin. Phys. B, 2017, 26 (**11**): 115204. DOI: 10.1088/1674-1056/26/11/115204

Generation of high quality ion beams through the stable radiation pressure acceleration of the near critical density target

Xue-Ren Hong(洪学仁), Wei-Jun Zhou(周伟军), Bai-Song Xie(谢柏松), Yang Yang(杨阳), Li Wang(王莉), Jian-Min Tian(田建民), Rong-An Tang(唐荣安), Wen-Shan Duan(段文山)
Chin. Phys. B, 2017, 26 (**6**): 065203. DOI: 10.1088/1674-1056/26/6/065203

Pulse chirping effect on controlling the transverse cavity oscillations in nonlinear bubble regime

H Vosoughian, Z Riazi, H Afarideh, G Sarri
Chin. Phys. B, 2017, 26 (**2**): 025201. DOI: 10.1088/1674-1056/26/2/025201

Developments in laser wakefield accelerators: From single-stage to two-stage

Li Wen-Tao, Wang Wen-Tao, Liu Jian-Sheng, Wang Cheng, Zhang Zhi-Jun, Qi Rong, Yu Chang-Hai, Li Ru-Xin, Xu Zhi-Zhan
Chin. Phys. B, 2015, 24 (**1**): 015205. DOI: 10.1088/1674-1056/24/1/015205

Optimization of the beam quality in ionization injection by a tailoring gas profile*

Ye Cui(崔野)[1], Guo-Bo Zhang(张国博)[1,†], Yan-Yun Ma(马燕云)[2,3,‡], Xiao-Hu Yang(杨晓虎)[1,3], Jia-Yin Mu(牟佳胤)[1], Hai-Bo Yao(姚海波)[1], Ming Zi(资明)[1], Jie Zhou(周洁)[4], Jing-Qi Yang(杨静琦)[4], Li-Xiang Hu(胡理想)[1], and Li-Chao Tian(田立朝)[1]

[1] *College of Liberal Arts and Sciences, National University of Defense Technology, Changsha* 410073, *China*
[2] *College of Advanced Interdisciplinary Studies, National University of Defense Technology, Changsha* 410073, *China*
[3] *Collaborative Innovation Center of IFSA (CICIFSA), Shanghai Jiao Tong University, Shanghai* 200240, *China*
[4] *XLAB, The Second Academy of CASIC, Beijing* 100854, *China*

(Received 3 June 2021; revised manuscript received 27 July 2021; accepted manuscript online 7 August 2021)

A new scheme is proposed to improve the electron beam quality of ionization-induced injection by tailoring gas profile in laser wakefield acceleration. Two-dimensional particle-in-cell simulations show that the ionization-induced injection mainly occurs in high-density stage and automatically truncates in low-density stage due to the decrease of the wakefield potential difference. The beam loading can be compensated by the elongated beam resulting from the density transition stage. The beam quality can be improved by shorter injection distance and beam loading effect. A quasi-monoenergetic electron beam with a central energy of 258 MeV and an energy spread of 5.1% is obtained under certain laser–plasma conditions.

Keywords: laser wakefield acceleration, ionization-induced injection, the beam loading effect

PACS: 52.38.Kd, 52.65.Rr, 52.35.Mw **DOI:** 10.1088/1674-1056/ac1b89

1. Introduction

Charged particle beams have potential applications in the areas of exploring microscopic material and the basic components of nature and universe, which are mainly produced by large-scale conventional radio-frequency (RF) accelerators under the current scientific and technological conditions.[1] But the material breakdown threshold limits the achievable acceleration gradient of RF accelerators to a few tens of MeV/m. The laser wakefield acceleration (LWFA) may become a promising technology for the next generation table-top accelerators in the future due to the tremendous acceleration gradient which usually can be as large as one thousand times of that of the traditional RF accelerators.[2] With the development of the chirped pulse amplification technology,[3] the laser intensity rapidly increases to the relativistic level, and provides favorable opportunities for LWFA.[4–6] In the nonlinear case, the laser excites cavitation regime, and this is so-called "bubble", which is benefical to obtaining monoenergetic electron beams.[7–9] Recently, the electron beams with monoenergetic peak up to 7.8 GeV have been demonstrated experimentally.[10]

Although the LWFA has ultrahigh acceleration gradient, the beam quality obtained from LWFA is not as good as that from RF accelerators. In LWFA, controlled electron injection is a key factor to improve electron beam quality. The electron injection means that the moving electrons locate at the accelerating phase of wakefield and are accelerated to high energy.[1] Many effective injection methods have been proposed to achieve this goal, e.g., colliding pulses injection,[11,12] density gradient injection,[13,14] and ionization-induced injection.[15,16] The ionization-induced injection is a typical longitudinal injection, which has been widely used in experiments due to the advantages of simple operation and controllability.[17,18] The monoenergetic electron beams with GeV energy by using this method have been obtained in recent years.[19,20] Such compact high quality electron sources have many applications in betatron radiation source,[21,22] ultrafast electron diffraction,[23,24] and free electron laser.[25] When an ultra-intense laser propagates through the mixture gas of high-Z and low-Z, the outer-shell electrons are ionized instantaneously and form plasma wakefield. The electrons in the inner-shell of high-Z atoms with higher ionization potential are released near the peak electric field of the laser pulse, and then they are preliminarily accelerated during the backward slippage. If the longitudinal velocity of these electrons exceeds the phase velocity of the wakefield, they could be trapped by the wakefield and accelerated to higher energy.[26,27] In the current experiments of LWFA, the laser

*Project supported by the National Natural Science Foundation of China (Grant Nos. 12005297, 11975308, and 11775305), the Strategic Priority Research Program of Chinese Academy of Sciences (Grant No. XDA25050200), the Fund of Science Challenge Project (Grant No. TZ2018001), Natural Science Foundation of Hunan Province, China (Grant No. 2020JJ5651), and the Fund of the State Key Laboratory of Laser Interaction with Matter (Grant No. SKLLIM1908).

†Corresponding author. E-mail: zgb830@163.com
‡Corresponding author. E-mail: plasim@163.com

© 2021 Chinese Physical Society and IOP Publishing Ltd

intensity is usually greater than the ionization threshold of the inner-shell electrons during the whole acceleration process due to the self-focusing effect, which leads to the continuous injection.[27,28] This phenomenon increases the difference of the ionized electrons not only in phase space, but also in actual acceleration distance, which results in high energy spread. In order to overcome these disadvantages, many schemes have been proposed to improve the beam quality of ionization injection.[29–31] However, more simple and efficient schemes of ionization injection are still necessary.

In this paper, we propose a scheme to improve the electron beam quality by tailoring the gas profile in ionization injection. We find that the ionization injection mainly occurs in high-density stage and truncates in low-density stage due to the decrease of the wakefield potential difference. Two-dimensional (2D) particle-in-cell (PIC) simulations reveal that the effective injection distance is controlled by the length of the high-density stage. Meanwhile, the longitudinal density profile of the injected electron beams can be modulated by the density transition stage, which can compensate for the beam loading effect.[32] Finally, the quality of the electron beam is improved. A quasi-monoenergetic electron beam with central energy of 258 MeV and energy spread of 5.1% is obtained under the simulated parameter conditions.

2. Simulation model

To analyze the process of the ionization-induced injection in multi-staged gas, 2D PIC simulations were performed in cartesian coordinates by using the LAPINE code.[33,34] A linearly polarized Gaussian laser propagates along z-axis from the left boundary of the simulation box with a wavelength of $\lambda_0 = 0.8$ μm, the spot radius of $w_0 = 15$ μm, the pulse duration of $\tau_L = 33$ fs. The normalized vector potential of the laser pulse is $a_0 = eE_{L0}/m_e\omega_0 c = 1.8$ where e is the electron charge, E_{L0} is the peak electric field, m_e is the rest electron mass, $\omega_0 = 2\pi c/\lambda_0$ is the laser frequency, and c is the speed of light, which corresponds to the pulse energy of 2.25 J. The simulation box with a size of 60 μm×100 μm is employed and moves along z-axis at the speed of light in vacuum. The simulation box is divided into 3000×1000 cells, and the size of each cell is 0.02 μm×0.1 μm. The time step is $\Delta t = 0.05$ fs to satisfy the courant condition. The on-axis electron density distribution is shown in Fig. 1. The background electrons come from the fully ionized hydrogen and the outer shell of neutral nitrogen. Because these electrons are bounded with low ionization potential and could be released near the leading edge of the laser. The main pulse directly interacts with N^{5+} ions rather than neutral nitrogen atoms. The density of nitrogen ions N^{5+} is $n_N = 1.4 \times 10^{16}$ cm^{-3}, which are considered as the injection source. According to the density distribution of the background electrons, the mixed plasma is divided into the high-density stage L_1, the density transition stage L_2, and the low-density stage L_3 respectively. There is also a density ramp from vacuum to uniform plasma with a length of 50 μm and the laser focuses at the front of the mixed plasma. It is worth mentioning that such density profile can be generated via double gas jets with different pressure in experiments.[13]

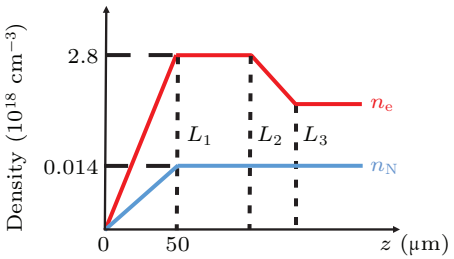


Fig. 1. Sketch of electron density n_e (red line) and neutral nitrogen ions n_N (blue line). The lengths of high-density stage, density transition stage, and low-density stage are represented by $L_{1,2,3}$ respectively.

3. Results and discussion

To illustrate the validity of our scheme, we firstly choose a group of typical parameters with the high-density stage of $L_1 = 450$ μm, the density transition stage of $L_2 = 100$ μm, and the low-density stage of $n_3 = 2.3 \times 10^{18}$ cm^{-3}. In our scheme, the laser intensity cannot trigger self-injection of the background electrons. Besides, the density gradient injection cannot occur due to small density gradient in the density transition stage. Therefore, the ionization-induced injection dominates and all trapped electrons come from the inner shell of nitrogen ions N^{5+}, which has been verified by the electron trajectories. The ionization injected electrons are accelerated to the dephasing position. Meanwhile, the case without density transition is also presented for comparison. Figure 2 shows the energy spectra of the accelerated electron beams with (red line) and without (blue line) the tailored profile at $t = 15.2$ ps. The electron beams have reached the dephasing position at this moment. We can see that the energy spectra without the density transition is platform-like. However, a quasi-monoenergetic electron beam with central energy of 258 MeV, maximum energy of 295 MeV, and energy spread of 5.1% is finally obtained for the case with the tailored profile.

In the ionization injection, the wakefield potential is a key factor to determine the ionization injection. In previous studies, the ionization injection condition has been presented and the potential difference between the initial ionization position and the minimum value satisfies $\Delta\Psi = 1$. Figures 3(a) and 3(c) show that the electron density distributions of the background plasma and ionized electrons at different time. $t = 1.5$ ps corresponds to the moment of the laser in the high-density stage and $t = 2.1$ ps corresponds to the moment of the laser in the low-density stage. We can see that the size of bubble and the length of the electron beam are a little elongated longitudinally, which are attributed to the fact that when the laser

propagates through the density transition regime, the plasma wavelength gets longer according to the equation $\lambda_p[\mu m] = 3.3\times10^{10}/\sqrt{n_e[cm^{-3}]}$ since the electron density n_e decreases. Figures 3(b) and 3(d) show the corresponding laser electric field and the wakefield potential difference between the initial ionization position and the minimum value. It can be seen that the laser has almost the same intensity profile at $t = 1.5$ ps and $t = 2.1$ ps. The change of the wakefield potential is mainly determined by the plasma density rather than the laser intensity. The minimum potential increases as the plasma density increases, which results in smaller potential difference. The potential difference decreases from $\Delta\Psi = 1.05$ at $t = 1.5$ ps to $\Delta\Psi = 0.95$ at $t = 2.1$ ps. The injection condition $\Delta\Psi \geq 1$ is no longer satisfied and truncates the ionization injection. The effective injection distance is reduced to a few hundred microns.

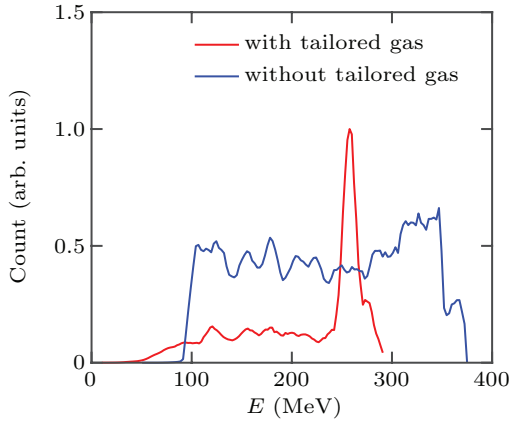


Fig. 2. Energy spectra of the accelerated electron beams with (red line) and without (blue line) tailored profile at $t = 15.2$ ps.

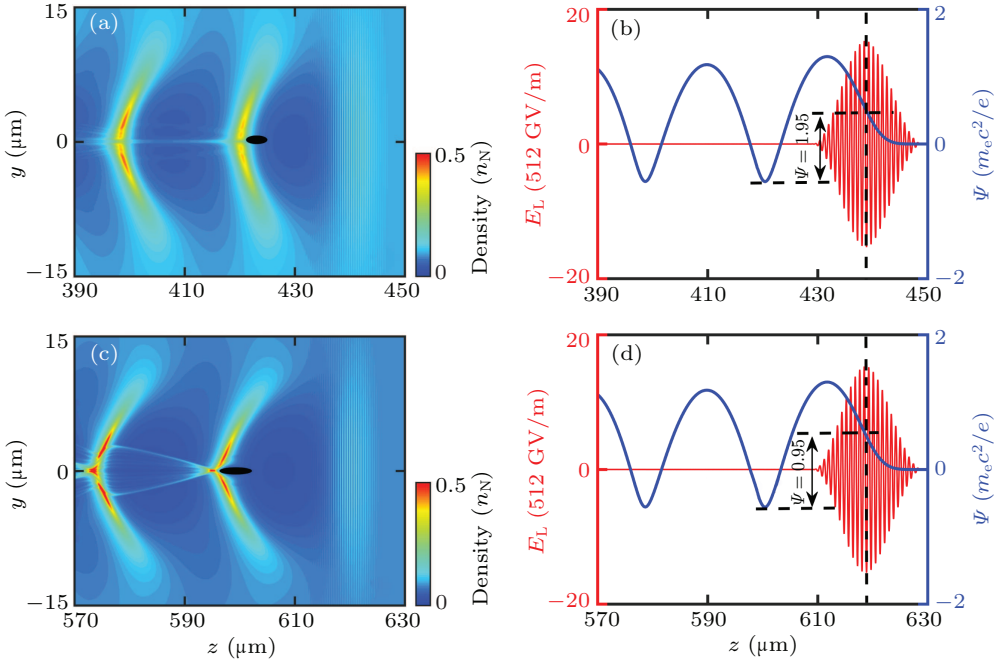


Fig. 3. Electron density distribution of background plasma and ionized electrons at $t = 1.5$ ps (a) and $t = 2.1$ ps (c). Panels (b) and (d) are the corresponding laser field (red line) and wakefield potential (blue line) along $y = 0$. The arrow represents the potential difference between the initial ionization position of the electrons and the minimum value.

In addition to the shorter injection distance, the density profile of the injected electron beam can compensate for the beam loading effect, which could affect the final beam quality. To study the effect of the electron injection process on the beam density profile, the transverse focusing field distribution and the injected electron trajectories are shown in Fig. 4. We can see that the shape of the transverse focusing field is almost identical to each other due to the small density difference. The injected electron trajectory in Fig. 4(a) comes from the high-density stage, while the one in Fig. 4(b) comes from the density transition stage. Along the laser propagation, plenty of off-axis electrons can be ionized and released. Although they satisfy the longitudinal ionization injection conditions $\Delta\Psi \geq 1$, they cannot be trapped and accelerated due to the large transverse velocity, as shown in Fig. 4(a). However, when the drive laser propagates through the density transition stage, as shown in Fig. 4(b), the size of the bubble gradually increases, e.g., $\propto n_e^{1/2}$, and the electrons have more time to decelerate transversely, which means relaxing the transverse trapping condition. Therefore, a large number of off-axis electrons are injected at the density transition stage, which significantly changes the density distribution of the injected electron beams. Figure 5 shows the density profile of the injected electron beams (red line) and the longitudinal accelerating field (blue line) at $y = 0$. In the density transition region, the intensity of the longitudinal acceleration field decreases while the plasma wavelength increases due to the reduced plasma density. As shown in Fig. 5(b), the optimized trapezoidal-shaped profile has a significant modulation on the wakefield due to the beam loading.[32] The longitudinal electric field E_z becomes

smooth. The whole electron beams get the same energy gain under the modulated wakefield. Therefore, the absolute energy spread would not increase due to excessive acceleration distance.

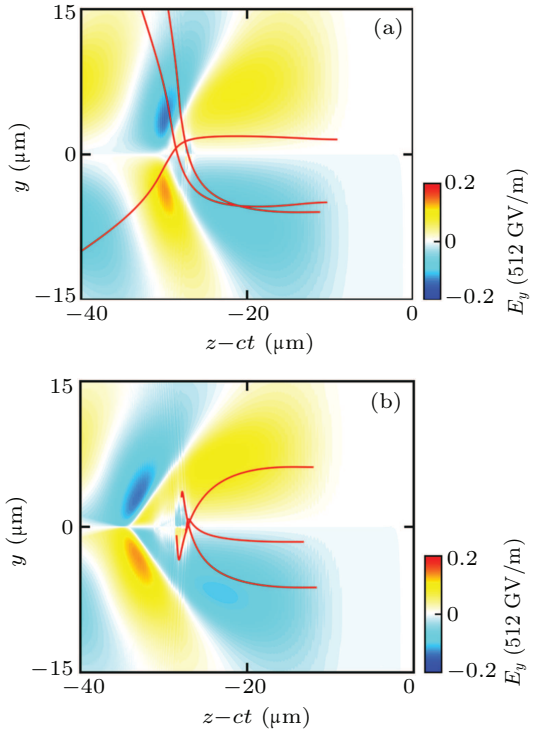


Fig. 4. Spatial distribution of the transverse focusing field E_y at $t =$ 1.5 ps (a) and $t = 2.1$ ps (b). Panel (a) is located in high-density stage and (b) is located in low-density stage. The red lines represent the injection electron trajectories in the wake rest frame $z - ct$.

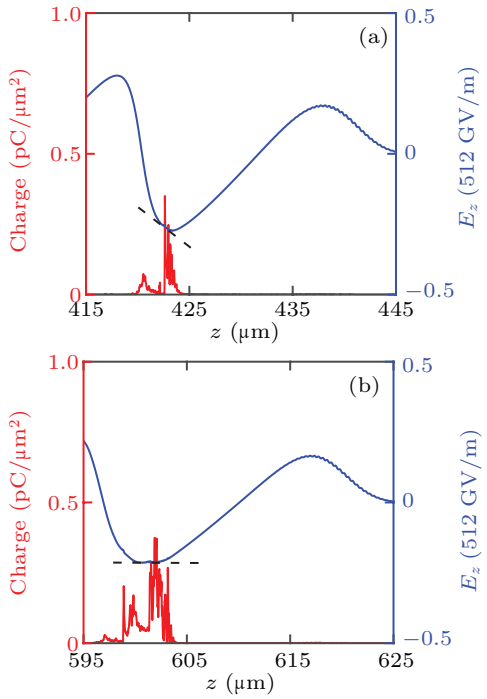


Fig. 5. The density profile of the injected electron beam (red line) and the longitudinal accelerating field (blue line) at $y = 0$: (a) $t = 1.5$ ps and (b) $t = 2.1$ ps. The black-dash line is the slope approximation of the accelerating field near the injected electron beams.

In view of the influence of the plasma density profile on the quality of the ionization injection electron beams, a series of simulations have been performed. The evolution of the injected charge is shown in Fig. 6(a). It could be seen that the injected charge increases at the same rate before $z =$ 500 μm. When the laser propagates through the low-density stage L_3 ($z >$ 500 μm), the ionization-induced injection truncates earlier as the density n_3 decreases and meanwhile the injected charge gets fewer. The injected charge in the case of $n_3 = 2.54 \times 10^{18}$ cm^{-3} (black-circle line) is larger than that in the case of 1.70×10^{18} cm^{-3} (red-triangle line). Figure 6(b) shows the evolution of the peak energy and energy spread as a function of the density n_3 ($L_1 = 650$ μm and $L_2 = 100$ μm are fixed). The density n_3 is related to the minimum potential $\Psi_{\min}$. The lower density would lift the minimum potential $\Psi_{\min}$ more obviously and cause smaller potential difference $\Delta\Psi$. We can see that the peak energy E_{peak} is larger with the increasing density n_3 due to the stronger acceleration field. Although the ionization-induced injection truncates earlier, the electron beams gain more energy. However, if the density n_3 is too low (e.g., $n_3 = 1.70 \times 10^{18}$ cm^{-3}), the density profile of the electron beam cannot smooth the wakefield effectively, which would increase the energy spread. It is worth noting that the short effective injection distance is the direct reason of beam quality improvement for the low density n_3. If the density n_3 is much higher, the reason for the beam quality improvement is the beam loading rather than the shorter distance. Figure 6(c) shows the influence of the length of the high density stage L_1 ($L_2 = 100$ μm and $n_3 = 2.26 \times 10^{18}$ cm^{-3} are fixed). If the length L_1 is too short (e.g., $L_1 = 150$ μm or 300 μm), the electron beam has lower charge, and the acceleration field could not be modulated to a trapezoidal-shaped profile in this case. Only when the injected charge in transition and high-density stages is approximately equal, the energy spread is obviously decreased via the beam loading effect. Figure 6(d) shows the evolution of the beam quality as a function of the length of the density transition stage ($L_1 = 450$ μm and $n_3 = 2.26 \times 10^{18}$ cm^{-3} are fixed). The difference of the electron energy is small with the change of L_2. The density gradient $(n_1 - n_3)/L_2$ determines the velocity of bubble elongation. As the length L_2 gets shorter, the velocity of the bubble bottom moves faster. More and more off-axis electrons can be injected. We can see that when the length of the density transition stage is between 100 μm and 200 μm, the energy spread of the electron beam is only about 5%. The electron energy would further increase with longer acceleration distance L_3.

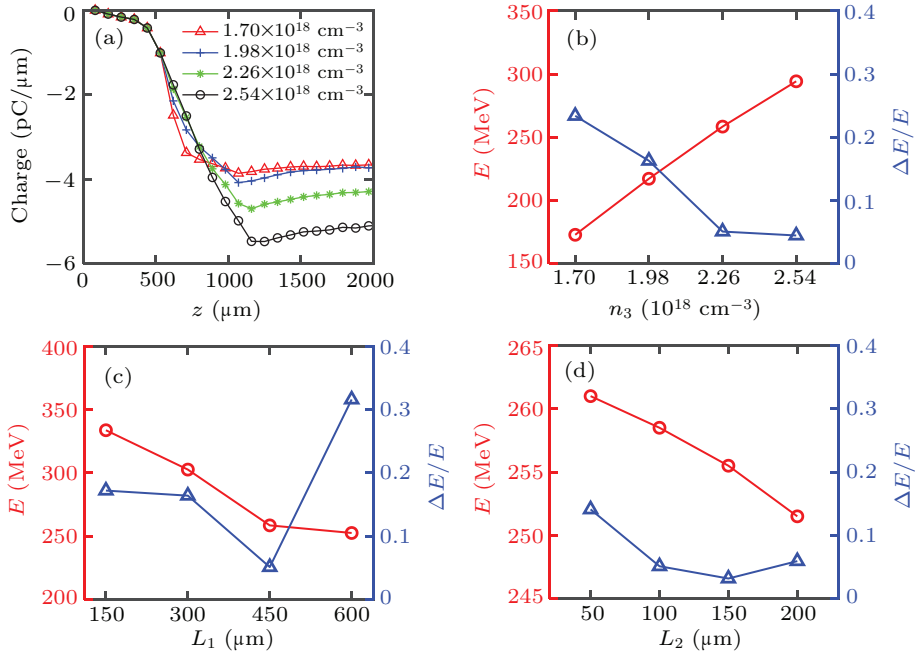


Fig. 6. (a) The evolution of injected charge as a function of the laser propagation. The peak energy and energy spread of the electron beam with tailored density profile at $t = 15.2$ ps as a function of the density n_3 (b); the length of high density stage L_1 (c); the length of the density transition stage L_2 (d).

It is mentioned that the ionization induced injection occurs in high-density stage L_1 and the density transition stage L_2. Then the injection truncates and the beams are accelerated to high energy in low-density stage L_3. The injected charge would increase if the length of L_1 and L_2 is increased. Besides, the charge and energy spread could be balanced by adjusting the lengths of different stages. The beam loading effect modulates the beam density distribution and smooths the wakefield, to make sure that the energy spread would not increase as the acceleration distance increases.

4. Conclusion

In this paper, we propose a new scheme to improve the electron beam quality of ionization-induced injection in laser wakefield acceleration. With tailored gas profile, the ionization-induced injection mainly occurs in the high-density stage and automatically truncates in the low-density stage due to the decrease of the wakefield potential difference, which effectively shortens the injection distance. What is more, the beam loading is compensated by the elongated electron beam from the off-axis electron injection in the density transition regime, and further improves the quality of the electron beam. As a result, a monoenergetic electron beam with central energy of 258 MeV and energy spread of 5.1% is finally obtained in two-dimensional simulations.

References

[1] Esarey E, Schroeder C B and Leemans W P 2009 *Rev. Mod. Phys.* **81** 1229
[2] Tajima T and Dawson J M 1979 *Phys. Rev. Lett.* **43** 267
[3] Strickland D and Mourou G 1985 *Opt. Commun.* **55** 447
[4] Faure J, Glinec Y, Pukhov A, Kiselev S, Gordienko S, Lefebvre E, Rousseau J P, Burgy F and Malka V 2004 *Nature* **431** 541
[5] Geddes C G R, Toth C, Van T J, Esarey E, Schroeder C B, Bruhwiler D, Nieter C, Cary J and Leemans W P 2004 *Nature* **431** 538
[6] Mangles S P D, Murphy C D, Najmudin Z, Thomas A G R, Collier J L, Dangor A E, Divall E J, Foster P S, Gallacher J G, Hooker C J, Jaroszynski D A, Langley A J, Mori W B, Norreys P A, Tsung F S, Viskup R, Walton B R and Krushelnick K 2004 *Nature* **431** 535
[7] Zhang G B, Chen M, Schroeder C B, Luo J, Zeng M, Li F Y, Yu L L, Weng S M, Ma Y Y, Yu T P, Sheng Z M and Esarey E 2016 *Phys. Plasmas* **23** 033114
[8] Lu W, Huang C, Zhou M, Mori W B and Katsouleas T 2006 *Phys. Rev. Lett.* **96** 165002
[9] Lu W, Huang C, Zhou M, Tzoufras M, Tsung F S, Mori W B and Katsouleas T 2006 *Phys. Plasmas* **13** 056709
[10] Gonsalves A J, Nakamura K, Daniels J, Benedetti C, Pieronek C, de Raadt T C H, Steinke S, Bin J H, Bulanov S S, van Tilborg J, Geddes C G R, Schroeder C B, Tóth C, Esarey E, Swanson K, Fan-Chiang L, Bagdasarov G, Bobrova N, Gasilov V, Korn G, Sasorov P and Leemans W P 2019 *Phys. Rev. Lett.* **122** 084801
[11] Faure J, Rechatin C, Norlin A Lifschitz A, Glinec Y and Malka V 2006 *Nature* **444** 737
[12] Kotaki H, Daito I, Kando M, Hayashi Y, Kawase K, Kameshima T, Fukuda Y, Homma T, Ma J, Chen L M, Esirkepov T Z, Pirozhkov A S, Koga J K, Faenov A, Pikuz T, Kiriyama H, Okada H, Shimomura T, Nakai Y, Tanoue M, Sasao H, Wakai D, Matsuura H, Kondo S, Kanazawa S, Sugiyama A, Daido H and Bulanov S V 2009 *Phys. Rev. Lett.* **103** 194803
[13] Geddes C G R, Nakamura K, Plateau G R, Toth C, Cormier-Michel E, Esarey E, Schroeder C B, Cary J R and Leemans W P 2008 *Phys. Rev. Lett.* **100** 215004
[14] Ke L T, Yu C H, Feng K, Qin Z Y, Jiang K N, Wang H, Luan S X, Yang X J, Xu Y, Leng Y X, Wang W T, Liu J S and Li R X 2021 *Appl. Sci.* **11** 2560
[15] Oz E, Deng S, Katsouleas T, Muggli P, Barnes C D, Blumenfeld I, Decker F J, Emma P, Hogan M J, Ischebeck R, Iverson R H, Kirby N, Krejcik P, O'Connell C, Siemann R H, Walz D, Auerbach D, Clayton C E, Huang C, Johnson D K, Joshi C, Lu W, Marsh K A, Mori W B and Zhou M 2007 *Phys. Rev. Lett.* **98** 084801
[16] Pak A, Marsh K A, Martins S F, Lu W, Mori W B and Joshi C 2010 *Phys. Rev. Lett.* **104** 025003
[17] Mirzaie M, Li S, Zeng M, Hafz N A M, Chen M, Li G Y, Zhu Q J, Liao H, Sokollik T, Liu F, Ma Y Y, Chen L M, Sheng Z M and Zhang J 2015 *Sci. Rep.* **5** 14659

[18] McGuffey C, Thomas A G R, Schumaker W, Matsuoka T, Chvykov V, Dollar F J, Kalintchenko G, Yanovsky V, Maksimchuk A, Krushelnick K, Bychenkov V Yu, Glazyrin I V and Karpeev A V 2010 *Phys. Rev. Lett.* **104** 025004
[19] Clayton C E, Ralph J E, Albert F, Fonseca R A, Glenzer S H, Joshi C, Lu W, Marsh K A, Martins S F, Mori W B, Pak A, Tsung F S, Pollock B B, Ross J S, Silva L O and Froula D H 2010 *Phys. Rev. Lett.* **105** 105003
[20] Liu J S, Xia C Q, Wang W T, Lu H Y, Wang C, Deng A H, Li W T, Zhang H, Liang X Y, Leng Y X, Lu X M, Wang C, Wang J Z, Nakajima K, Li R X and Xu Z Z 2011 *Phys. Rev. Lett.* **107** 035001
[21] Fuchs M, Weingartner R, Popp A, Major Z, Becker S, Osterhoff J, Cortrie I, Zeitler B, Hörlein R, Tsakiris G D, Schramm T U, Rowlands-Rees T P, Hooker S M, Habs D, Krausz F, Karsch S and Grüner F 2009 *Nat. Phys.* **5** 826
[22] Zhang G B, Chen M, Yang X H, Liu F, Weng S M, Ma Y Y, Zou D B, Yu T P, Shao F Q and Sheng Z M 2020 *Opt. Express* **28** 29927
[23] Sciaini G and Miller R J D 2011 *Rep. Prog. Phys.* **74** 096101
[24] Faure J, van der Geer B, Beaurepaire B, Gallé G, Vernier A and Lifschitz A 2016 *Phys. Rev. Accel. Beams* **19** 021302
[25] Nakajima K 2008 *Nat. Phys.* **4** 92
[26] Chen M, Sheng Z M, Ma Y Y and Zhang J 2006 *J. Appl. Phys.* **99** 056109
[27] Chen M, Esarey E, Schroeder C B, Geddes C G R and Leemans W P 2012 *Phys. Plasmas* **19** 033101
[28] Sun G Z, Ott E, Lee Y C and Guzdar P 1987 *Phys. Fluids* **30** 526
[29] Yu L L, Esarey E, Schroeder C B, Vay J L, Benedetti C, Geddes C G R, Chen M and Leemans W P 2014 *Phys. Rev. Lett.* **112** 125001
[30] Zhao Q, Weng S M, Sheng Z M, Chen M, Zhang G B, Mori W B, Hidding B, Jaroszynski D A and Zhang J 2018 *New J. Phys.* **20** 063031
[31] Cui Y, Zhang G B, Ma Y Y, Zou D B, Yang X H, Chen M, Liu J X, Ge Z Y, Tian L C, Gan L F and Shao F Q 2019 *Plasma Phys. Contr. F.* **61** 085023
[32] Tzoufras M, Lu W, Tsung F S, Huang C, Mori W B, Katsouleas T, Vieira J, Fonseca R A and Silva L O 2009 *Phys. Plasmas* **16** 056705
[33] Yang X H, Dieckmann M E, Sarri G and Borghesi M 2012 *Phys. Plasmas* **19** 113110
[34] Xu H, Yu W, Yu M Y, Wong A Y, Sheng Z M, Murakami M and Zhang J 2012 *Appl. Phys. Lett.* **100** 144101